Volume 21
Number 39
21 October 2025
Pages 7575–7728

Soft Matter

rsc.li/soft-matter-journal

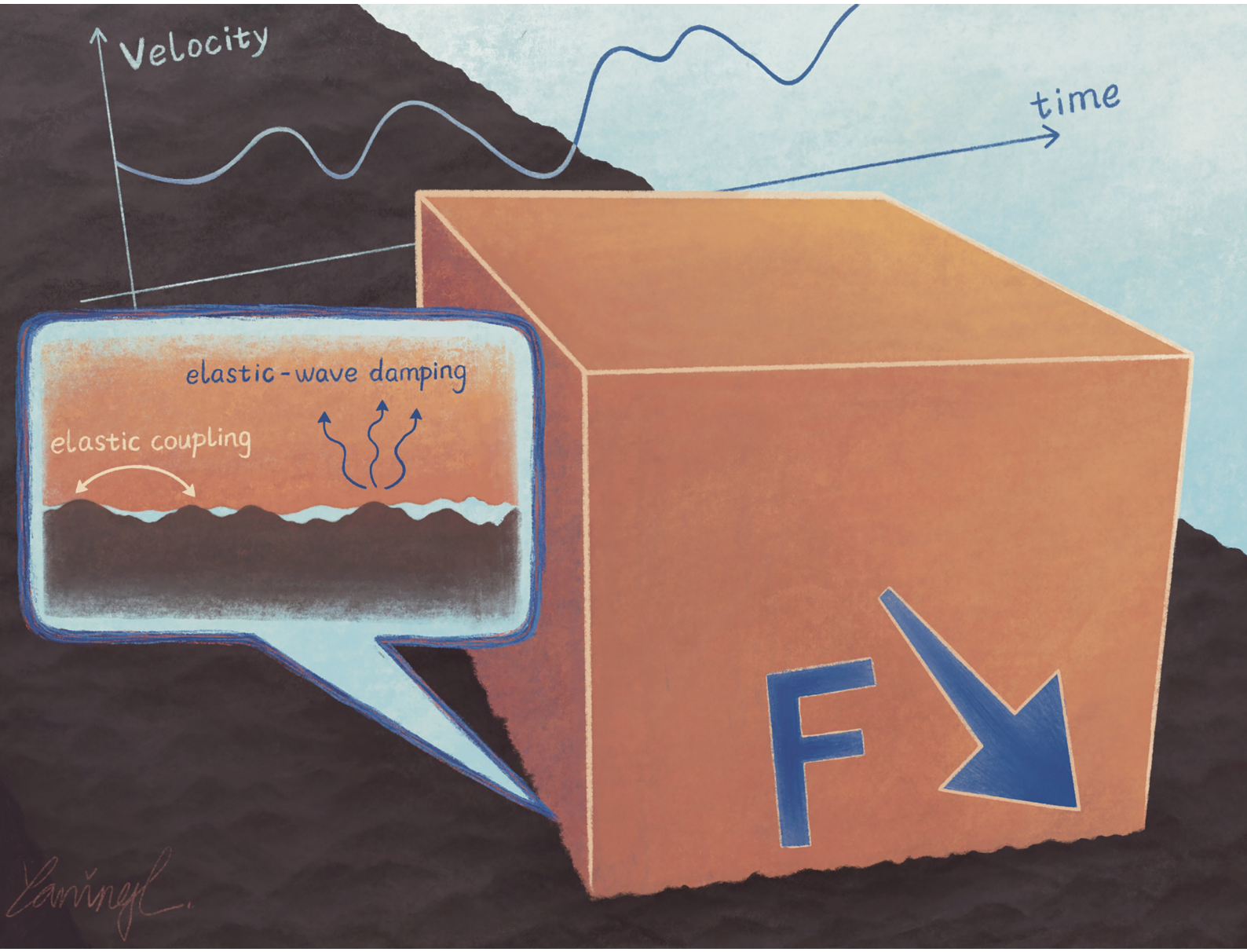

ISSN 1744-6848

ROYAL SOCIETY OF CHEMISTRY

PAPER
F. Zhou, B. N. J. Persson *et al.*
Friction dynamics: displacement fluctuations during sliding friction

20 YEARS ANNIVERSARY

Soft Matter

PAPER

View Article Online
View Journal | View Issue

Cite this: *Soft Matter*, 2025, **21**, 7594

Friction dynamics: displacement fluctuations during sliding friction

R. Xu, [abc] F. Zhou [*a] and B. N. J. Persson [*abc]

We have investigated the fluctuations (noise) in the positions of rectangular blocks, made from rubber or polymethyl methacrylate (PMMA), sliding on various substrates under constant driving forces. For all systems the power spectra of the noise exhibit large low-frequency regions with power laws, $\omega^{-\gamma}$, with the exponents γ between 4 and 5. The experimental results are compared to simulations and analytical predictions using three models of interfacial interaction: a spring-block model, an asperity-force model, and a wear-particle model. In the spring-block model, small sub-blocks (representing asperity contact regions) are connected to a larger block *via* viscoelastic springs and interact with the substrate through forces that fluctuate randomly in both time and magnitude. This model gives a power law with $\gamma = 4$, as also observed in experiments when no wear particles can be observed. The asperity-force model assumes a smooth block sliding over a randomly rough substrate, where the force acting on the block fluctuates in time because of fluctuations in the number and size of contact regions. This model predicts a power law with the exponent $\gamma = 6$, which disagrees with the experiments. We attribute this discrepancy to the neglect of load redistribution among asperity contacts as they form or disappear. The wear-particle model considers the irregular dynamics of wear particles of varying sizes moving at the interface. This model also predicts power-law power spectra but the exponent depends on two trapping-release probability distributions. If chosen suitably it can reproduce the exponent $\gamma = 5$ (which corresponds to $1/f$ noise in the friction force) observed in some cases.

Received 18th June 2025,
Accepted 26th July 2025

DOI: 10.1039/d5sm00617a

rsc.li/soft-matter-journal

1 Introduction

All solid surfaces exhibit roughness extending over many decades in length scale.[1–3] When two solids come into contact, they generally touch only a small fraction of the nominal contact area where asperities make contact.[4–10] The asperity contact regions may undergo stick-slip motion during sliding, which can be correlated due to elastic coupling between different regions.[11–15] The stick-slip motion depends on the nature of surface roughness, which can induce nearly random fluctuations (noise) in the sliding distance.

Fluctuations in sliding friction have been studied previously using two different methods. One method involves driving the slider at a constant speed and analyzing fluctuations in the driving force.[16] However, accurately measuring forces is challenging, making this method suitable only for systems with relatively large force fluctuations. Another method involves detecting and analyzing the sound waves emitted from the sliding junction.[17,18] However, correlating the sound wave frequency spectra to the motion or the friction force acting on the block, is not straightforward.

In a previous paper,[19] we proposed a new approach to study sliding dynamics by applying a constant driving force and analyzing the fluctuations in the position of the block. The advantage is that, compared to force, distances can be measured accurately using various methods, with one extreme example being the laser displacement sensors used for studying gravitational waves, capable of measuring changes in distances down to $\sim 10^{-4}$ of the width of a proton.[20] In the experiments, solid blocks were slid on nominally flat surfaces with different roughness. If the average velocity of the center of mass of a block is denoted by v, the sliding distance $s = vt + \xi(t)$, where $\xi(t)$ is the random fluctuation away from the mean (ensemble averaged) block position. From the obtained $\xi(t)$, the displacement (position) power spectra were calculated. Simulations using a simple block-spring model yielded good agreement with experimental results.

In this paper, we extend the study in ref. 19. In addition to the two rubber blocks (compounds A and B) used in ref. 19, we introduce a PMMA block. As substrates, we include a tile surface alongside the concrete and smooth glass surfaces used previously. The distance (or time) sampling frequency is

[a] *State Key Laboratory of Solid Lubrication, Lanzhou Institute of Chemical Physics, Chinese Academy of Sciences, 730000 Lanzhou, China*
[b] *Peter Grünberg Institute (PGI-1), Forschungszentrum Jülich, 52425 Jülich, Germany. E-mail: b.persson@fz-juelich.de*
[c] *MultiscaleConsulting, Wolfshovener str. 2, 52428 Jülich, Germany*

optimized to capture higher-frequency noise than in the previous study. In addition to the displacement power spectra, the force power spectra are also calculated based on the obtained $\xi(t)$.

We present simulations and analytical studies using three different models: (I) the block-spring model from ref. 19, (II) a wear particle model, and (III) an asperity force model. For models (I) and (II), we derive analytical expressions for how the power spectra depend on the sliding block velocity and other parameters.

The results indicate that for all models, there exist broad frequency regions where the sliding distance and force power spectra follow power-law behavior. The exponents predicted by models (I) and (II) align with experimental results, whereas model (III) fails to provide an accurate description. The failure of model (III) arises from its inability to account for the redistribution of load among asperities when the block moves into or out of contact with a single asperity. Including this effect would change the time series for the friction force but would also make the fluctuations in the force much smaller.

The mechanisms explored in this study, namely the stochastic formation and rupture of asperity contacts and the resulting force fluctuations, are relevant to a broad range of physical systems beyond the current experimental setup. In particular, similar processes underlie models of earthquake dynamics, such as rate-and-state friction,[21–25] where the evolution of microscopic contact regions governs macroscopic stick-slip behavior. Analogous interfacial phenomena are also important in sliding electrical contacts, including those in railway power systems,[26–28] and in the generation of friction-induced acoustic noise in mechanical and structural applications.[17,18,29]

2 Sliding distance and force power spectra

Part of the following derivation was given in the earlier study,[19] but it is included here for completeness. The equation of motion for the block is given by

$$M\frac{\mathrm{d}^2x}{\mathrm{d}t^2} = F_{\mathrm{drive}} + F,$$

where $F = -Mg\mu(t)$ is the friction force.

We express $x(t) = vt + \xi(t)$ and $F(t) = F_0(v) + F_1(t)$ and choose F_0 so that $F_{\mathrm{drive}} = F_0$. This gives

$$M\frac{\mathrm{d}^2\xi}{\mathrm{d}t^2} = F_1(t) \tag{1}$$

We define the displacement power spectrum as

$$C_x(\omega) = \frac{1}{2\pi}\int_{-\infty}^{\infty}\mathrm{d}t\langle\xi(t)\xi(0)\rangle\mathrm{e}^{i\omega t} \tag{2}$$

The power spectrum can also be expressed as

$$C_x(\omega) = \frac{2\pi}{T}|\xi(\omega)|^2,$$

where T is the total sliding time and

$$\xi(\omega) = \frac{1}{2\pi}\int_{-T/2}^{T/2}\mathrm{d}t\xi(t)\mathrm{e}^{-i\omega t}.$$

Using eqn (1), we obtain

$$-M\omega^2\xi(\omega) = F_1(\omega),$$

thus

$$C_x(\omega) = \frac{2\pi}{T}|\xi(\omega)|^2 = \frac{2\pi}{T}|F_1(\omega)|^2\frac{1}{M^2\omega^4} = \frac{1}{M^2\omega^4}C_{\mathrm{F}}(\omega).$$

Therefore, the power spectrum of the friction force is

$$C_{\mathrm{F}}(\omega) = M^2\omega^4C_x(\omega) \tag{3}$$

In a similar way, writing the friction coefficient as $\mu(t) = \mu_0(v) + \mu_1(t)$, and choosing μ_0 such that $F_{\mathrm{drive}} - Mg\mu_0 = 0$ gives

$$\frac{\mathrm{d}^2\xi}{\mathrm{d}t^2} = -g\mu_1(t).$$

Using this equation, we obtain

$$-\omega^2\xi(\omega) = -g\mu_1(\omega),$$

thus

$$C_x(\omega) = \frac{2\pi}{T}|\xi(\omega)|^2 = \frac{2\pi}{T}|\mu_1(\omega)|^2\frac{g^2}{\omega^4} = \frac{g^2}{\omega^4}C_\mu(\omega).$$

Therefore, the power spectrum of the friction coefficient is

$$C_\mu(\omega) = \frac{\omega^4}{g^2}C_x(\omega).$$

Instead of considering the sliding motion as a function of time, one could consider it as a function of the average sliding distance $s = vt$. The random displacement ξ can be considered as a function of the average distance $s = vt$ and can be Fourier decomposed into a sum of $\exp(iqs)$ waves with different amplitudes and wavenumber q. The advantage of this approach is that results for different sliding speeds may be very similar when considered as a function of s or q, because one expects the random forces acting in asperity contact regions to depend on the location of the rubber block on the substrate surface rather than on time, at least if thermal activation is unimportant. However, the same effect can be achieved by shifting the $C_x(\omega)$ spectra, measured at different sliding speeds, along the frequency axis.

From (2) we get

$$\langle\xi(t)\xi(0)\rangle = \int_{-\infty}^{\infty}\mathrm{d}\omega C_x(\omega)\mathrm{e}^{-i\omega t},$$

from which we obtain the mean-square (ms) displacement

$$\xi_{\mathrm{rms}}{}^2 = \left\langle[\xi(0)]^2\right\rangle = 2\int_0^{\infty}\mathrm{d}\omega C_x(\omega) \tag{4}$$

where we have used that $C_x(-\omega) = C_x(\omega)$. In a similar way, the ms value of the noise in the friction coefficient is given by

$$\mu_{\mathrm{rms}}{}^2 = \left\langle [\mu_1]^2 \right\rangle = 2\int_0^\infty \mathrm{d}\omega \frac{\omega^4}{g^2} C_x(\omega).$$

We have derived a relation (3) between the power spectra of the sliding distance and the friction force. One may ask under what conditions will measurements performed with a constant driving force (as done in this study) or a constant driving speed (as done in the study of ref. 16) give the same result. For the very low-frequency noise, which results from variation of the substrate surface properties over length scales larger than the size of the sliding block, the two cases will give different results which is clear in the limiting case where the local friction becomes so large as to stop the sliding in the case of a constant driving force. Similarly, for very small sliding blocks, where the asperity stick-slip motion may involve the whole bottom surface of the block, one would expect a difference between the two cases. However, for large systems, if the upper surface is moving at a constant speed the local slip events at the interface will, because of self averaging, give rise to a nearly constant sliding friction force. In this case assuming a constant driving force (which results in the same average sliding speed as in the constant sliding speed case) will result in the same distribution of slip events at the interface, and the same information will be contained in the (force or distance) noise spectra in both cases.

3 Model I: block-spring model

The spring-block model used in this work is based on the framework introduced in our earlier study,[19] in which a large elastic block is connected to N viscoelastic sub-blocks representing asperity contact regions. These sub-blocks are coupled *via* springs and dampers and are subjected to random forces originating from the substrate.

Fig. 1 illustrates the model: a large block of mass M is connected to N miniblocks of mass m *via* springs with stiffness k_0 and damping coefficient η_0. The miniblocks are also coupled laterally *via* springs with stiffness k_1 and damping coefficient η_1. Random lateral forces $f_i(t)$ act on the miniblocks, simulating the disordered interactions at the sliding interface. A schematic extension of the model to include smaller-scale microblocks is shown in Fig. 1(c), although these are not explicitly included in the simulations presented in this study.

The theory assumes that on the miniblocks in Fig. 1 act a kinetic friction force f_k and a randomly fluctuating forces $f_i(t)$ with a time average $\langle f_i \rangle = 0$. We assume that $f_i(t)$ changes randomly with the sliding distance at an average rate denoted as $1/a$. We set a equal to the typical diameter D of the macro asperity contact regions, as sliding over a distance D is expected to renew the asperity contacts. If the large block moves from x to $x + a$ during the time period Δt, the force on a miniblock (coordinate x_i) changes randomly between t and $t + \Delta t$ from its old value to

$$f_i = \alpha f_{\mathrm{kin}}(r_i - 0.5) \quad (5)$$

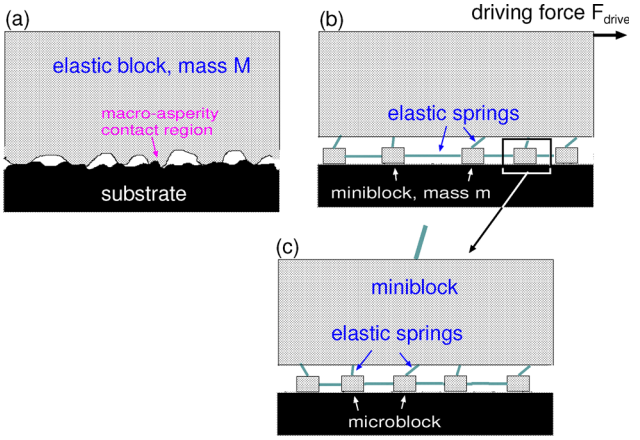

Fig. 1 A block-spring model. (a) The sliding block interacts with the substrate in N asperity contact regions randomly distributed at the interface. The asperities experience randomly fluctuating forces from the substrate. (b) The equivalent block-spring model. (c) Multiscale extension including microblocks. Note that the effects of microblocks are not included in the simulation results presented in this study.

where r_i is a random number uniformly distributed between 0 and 1, and α is a parameter expected to be of order 1. These random fluctuations in f_i are interpreted as resulting from changes in the contact between the asperities on the block and the substrate. The average frequency of fluctuations of the random force f_i is v/a. In Appendix A, we show that for $v/a \ll \omega \ll \omega_c$, we obtain:

$$C_x(\omega) \approx \frac{\alpha^2}{\omega^4} \frac{v^3}{12\pi N a} \quad (6)$$

The scaling $C_x \sim \omega^{-4}$ implies that the force power spectrum C_F is independent of frequency in the specified interval.

4 Simulation results for model I

In the simulations we assume $F_{\mathrm{drive}} = 10$ N and $F_{\mathrm{kin}} = Nf_{\mathrm{kin}} = 5$ N, where N is the total number of miniblocks. If D is the diameter of an asperity contact region theory predicts[30] that spring constant $k_0 \approx ED$. Using a rubber slider with $E \approx 10^7$ Pa and assuming a typical diameter $D \approx 1$ mm, we get $k_0 = 10^4$ N m^{-1}. The mass of the large block is $M = 1$ kg and the mass of a miniblock is assumed to be a few times $\rho D^3 \approx 10^{-6}$ kg; we use $m = 10^{-5}$ kg. The lateral coupling between the miniblocks depends on the separation between macroasperity contact regions. Assuming a separation of order D, we get $k_1 \approx k_0$, but as the separation is likely larger, we take $k_1 = 10^2$ N m^{-1}. However, simulations show that displacement power spectra are nearly the same for all $0 < k_1 < k_0$, so the exact value of k_1 is not critical for this study. The damping η_0 is chosen such that the vibrational motion of a contact region, if free, would be nearly overdamped, giving $\eta_0 \approx \sqrt{(k_0/m)}$; we use $\eta_0 = 0.8 \times 10^4$ s^{-1}. The damping η_1 determines the increase in friction force with increasing sliding speed. We compare the theory to experimental data obtained for an average speed of $v = 0.5$ mm s^{-1}, choosing η_1 so that the friction force equals F_{drive} at this

speed. The sliding distance needed to renew the contact regions is set to D, so a = 1 mm. The parameters above with $\alpha = 1$ and $N = 30$ are used as the "standard" or "reference" case. When parameters differ from this case, we will specify only the differing parameters.

We performed simulations of the spring-block model using the same parameter set as in ref. 19 (which was motivated by physical arguments), referred to as the "reference case": $N = 30$, $v = 0.5$ mm s^{-1}, $a = 1$ mm, $k_0 = 10^4$ N m^{-1}, $k_1 = 10^2$ N m^{-1}, $M = 1$ kg, $m = 10^{-5}$ kg, $\eta_0 = 0.8 \times 10^4$ s^{-1}, and $\alpha = 1$.

Fig. 2(a) shows the simulation results for the displacement power spectrum $C_x(\omega)$ in the reference case and for several variations, including increased sliding speed, decreased renewal length a, and increased number of miniblocks. Fig. 2(b) illustrates the effect of varying the noise strength parameter α. The spectra exhibit an ω^{-4} scaling over a broad frequency range, with the entire spectrum shifting to higher frequencies as the sliding speed increases as predicted by (6) (see also Appendix A).

The origin of the ω^{-4} behavior for $\omega < \omega_c$ has been discussed in detail in ref. 19, where it was shown that if the fluctuations in the friction force acting on the block are temporally uncorrelated on long time scales, the corresponding power spectrum $C_F(\omega)$ becomes independent of frequency for low ω, which result in $C_x(\omega) \sim \omega^{-4}$ according to (3). At high frequencies, $C_x(\omega)$ tends to flatten. As detailed in Appendix A, this behavior arises from the response of the large block to the damped oscillations of the miniblocks, which are driven by the random forces acting on them.

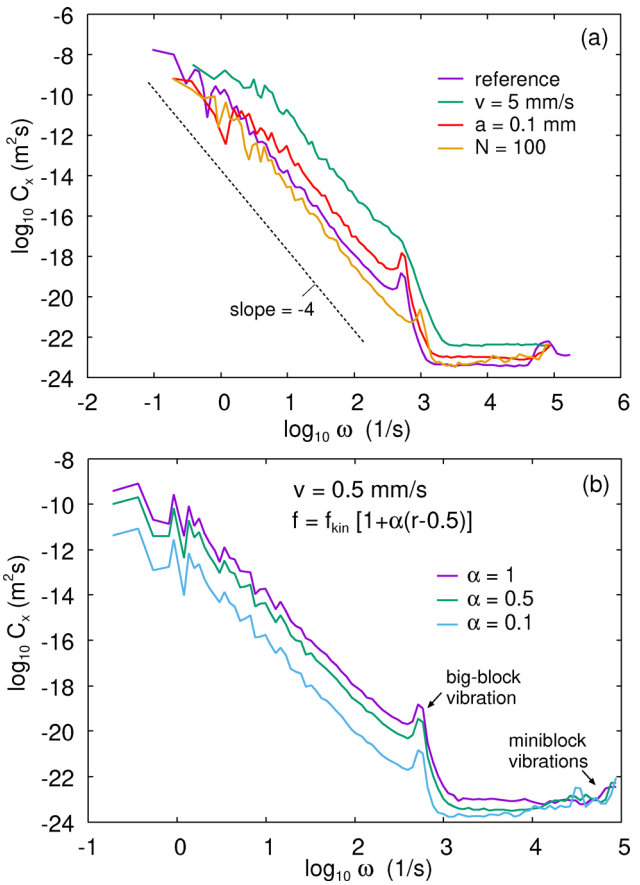

Fig. 2 (a) Displacement power spectrum $C_x(\omega)$ for different model parameters. (b) Effect of varying the noise strength parameter α on the power spectrum $C_x(\omega)$. Adapted from ref. 19.

5 Model II: wear particle model

If wear particles form, they could contribute to fluctuations in the sliding friction force. Wear particles may undergo irregular motion resulting from trap-and-release (or break-loose) processes that occur at variable rates (see Fig. 3). This may lead to fluctuations in the friction force with a ω^{-1} frequency dependence. This behavior is analogous to Schottky's original explanation of ω^{-1} noise in vacuum tubes, where he proposed that charge carriers become trapped in capture sites and are released at variable rates.[31–33] A similar effect may occur due to contamination particles (such as dust), which are always present on surfaces exposed to the normal atmosphere. Noise with a frequency spectrum proportional to ω^{-1}, often referred to as $1/f$ noise, is very common, although no generally accepted theory exists to explain its origin. In Appendix B, we present a simple model that resembles the one proposed for noise in vacuum tubes. However, this model only results in a ω^{-1} dependence under certain conditions.

6 Model III: asperity force model

Here we present a model that is simpler than the one studied in Section 3. We assume that the sliding block has a flat surface (no roughness), while the substrate has random roughness. When an asperity makes contact with the block at the leading (front) edge, it remains in contact and exerts a constant friction force on the block until it exits at the trailing edge; see Fig. 4. In this scenario, fluctuations in the force acting on the block result solely from stochastic fluctuations in the number of asperity contact regions and fluctuations in the size of those regions.

The friction force time series for the model shown in Fig. 4 is obtained as follows. Time is discretized into steps of length Δt. We choose Δt small enough that during this interval, at most

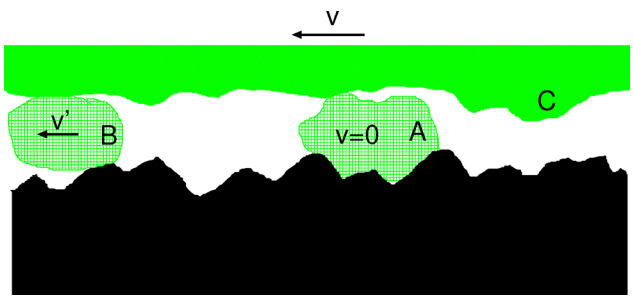

Fig. 3 A block (green) sliding with velocity v on a substrate with two wear particles. Particle B is moving relative to the substrate with velocity v', while particle A is trapped by the substrate's roughness. Particle A may be released (break loose) if asperity C collides with it.

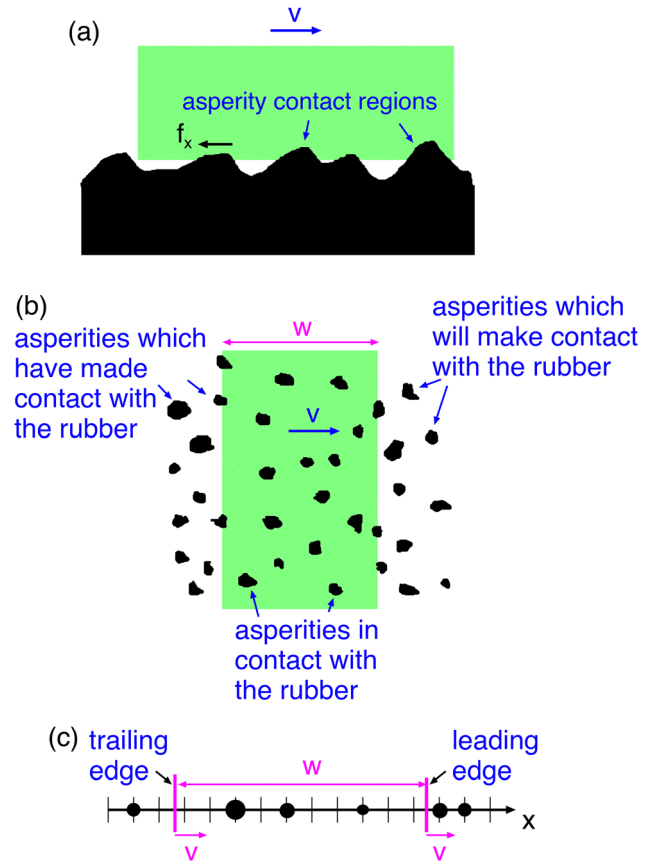

Fig. 4 (a) An elastic block with a flat bottom surface sliding on a rigid, randomly rough substrate. (b) An asperity that comes into contact with the block at the leading edge will remain in contact until the trailing edge, exerting a constant friction force f_x on the block. Here, we assume no local stick-slip at the asperity level. The total force acting on the block is the sum of the forces from each asperity contact region, fluctuating randomly in time due to random variations in the number and size of the asperity contact regions. (c) A one-dimensional (1D) model is used to calculate the force on the sliding block. All asperity contact regions are projected onto the x-axis, and the force acting on the block is determined by all the asperities between the moving (velocity v) vertical boundary lines separated by the width w of the block.

one new asperity contact is formed at the leading edge, and at most one asperity contact disappears at the trailing edge. The x-axis (in the sliding direction) is discretized into steps of length $\Delta x = v\Delta t$. We associate a random force $f(i)$ with each $x = i\Delta x$ grid point, where $f(i) = 0$ with the probability $1 - p$ and $f(i) = rf_0$ with the probability p, where r is a random number uniformly distributed between 0 and 1.

If w is the width of the block in the sliding direction, then there will be $N_w = w/\Delta x$ grid points within the width w. On average, there will be $N = pN_w = pw/\Delta x$ asperity contact regions, each exerting an average force $f_0/2$, giving a total average friction force $F_f = Nf_0/2 = pwf_0/(2\Delta x)$. The actual number of asperity contact regions will fluctuate in time, so that $F_x(t + \Delta t) = F_x(t) + f(i + N_w) - f(i)$. We obtain the displacement power spectrum $C_x(\omega)$ from the force power spectrum $C_F(\omega)$ using eqn (3).

7 Simulation results for model III

We present numerical results for the simulation of model III using the following parameters: $F_f = 5$ N, sliding speed $v = 0.5$ mm s^{-1}, and $p = 0.1$. The mass of the block is $M = 1$ kg and the width of the block in the sliding direction is $w = 1$ cm. An example of the simulated time-dependent friction force for $N = 30$ asperity contact regions is shown in Fig. 5.

Fig. 6 shows the displacement power spectrum as a function of frequency (log–log scale). Results are shown for $N = 30$ and $N = 300$ asperity contact regions. Note that the power spectrum $C_x \sim \omega^{-n}$ with $n = 6$, which is larger than the experimentally observed range of n between 4 and 5. Additionally, the power spectrum at low frequencies is larger than observed experimentally.

The reason this model fails to accurately describe reality is that when the block moves into or out of contact with an asperity, it alters the load carried by other asperities. Accounting

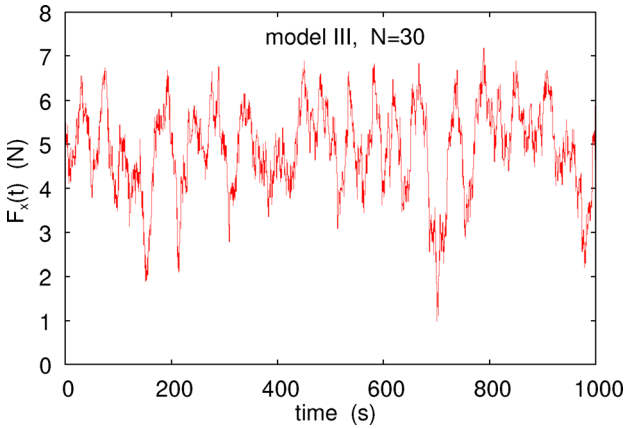

Fig. 5 The tangential (friction) force as a function of sliding time for (on average) $N = 30$ asperity contact regions.

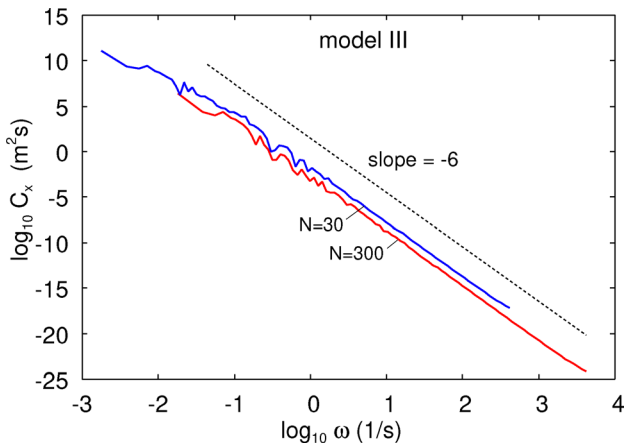

Fig. 6 The displacement power spectrum as a function of frequency (log–log scale). Results are shown for $N = 30$ and $N = 300$ asperity contact regions. The other parameters are $F_f = 5$ N, sliding speed $v = 0.5$ mm s^{-1}, and $p = 0.1$. The mass of the block is $M = 1$ kg and the width of the block in the sliding direction is $w = 1$ cm.

for this effect would reduce the magnitude of the fluctuations in the friction force acting on the block.

8 Experimental setup: Leonardo da Vinci slider

The experimental setup is similar to that used in ref. 19, and is shown in Fig. 7, where a displacement sensor tracks the position of the slider under constant driving force. The slider consists of two rubber or PMMA blocks glued to a wood plate, with one block positioned at the front and the other at the back. The nominal contact area is $A_0 \approx 10$ cm^2. The normal force F_N is determined by the total mass M of lead blocks placed on top of the wood plate. Similarly, the driving force is determined by the total mass M' of lead blocks in the container (the mass of the ropes are neglected).

The sliding distance $x(t)$ as a function of time t is measured using a Sony DK50NR5 displacement sensor with a resolution of 0.5 μm. This distance sensor does not exhibit any observable noise as evidenced by a flat, time-invariant signal when no sliding motion is present. This simple friction slider setup can also be used to calculate the friction coefficient $\mu = M'/M$ as a function of sliding velocity and nominal contact pressure $p = Mg/A_0$. Note that with this setup, the driving force is specified, allowing the study of the velocity dependence of friction only on the branch of the $\mu(v)$ curve where the friction coefficient increases with increasing speed.

We also performed some studies where instead of the set-up shown in Fig. 7 the substrate was put on a tilted (angle α) plane. In this case the driving force $Mg\sin\alpha$ and the normal force $Mg\cos\alpha$ are the tangential and normal parts of the gravitational force acting on the mass M. In all cases the force sensor was not in direct contact with the slider system and the slider was located on a stiff vibrational-isolated table and the experiments were performed in the basement of a building. Still we cannot exclude that some external vibrations may influence the results.

Both rubber compounds used in our studies are tire tread rubber consisting of styrene butadiene rubber with carbon black fillers, supplied by two different tire companies. Before the friction studies the rubber and PMMA surfaces were cleaned by soap water and dried. The glass surface was also cleaned by soap water, and all surfaces were cleaned by a soft brush between each sliding experiment to remove wear (and dust) particles. All the substrate surfaces have been used in earlier studies and their surface roughness power spectra were reported in ref. 34,35 citefootwear, concrete.

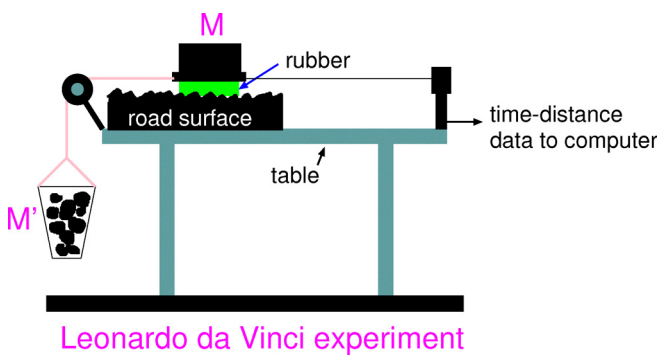

Fig. 7 A simple friction slider (schematic) measures the sliding distance $x(t)$ *via* a displacement sensor.

9 Experimental results

We have measured the sliding distance $x(t)$ for three different systems: one rubber block (compound A) sliding on a rough concrete, a smooth silica glass, and a tile surface; a second rubber block (compound B) sliding on concrete and glass surfaces; and a PMMA block sliding on concrete and tile surfaces. Experimental results for compound A on concrete and glass surfaces were originally presented in ref. 19. They are shown here for reference and comparison with new systems. All tests were conducted under different normal loads and driving forces. The experimental conditions are summarized in Tables 1–3.

Fig. 8 (top) shows the noise $\xi(t) = x(t) - vt$ of the block position as a function of time for compound B on concrete. The average sliding speed is $v = 0.054$ mm s^{-1} and the total sliding

Table 1 Experimental conditions for compound A sliding on concrete, glass, and tile

Rubber A – concrete				
No.	F_N [N]	F_{drive} [N]	μ [—]	v [μm s^{-1}]
1	32.86	14.26	0.43	16
2		17.74	0.54	37
3		18.66	0.57	101
	—			
4	60.72	22.08	0.36	2.24
5		39.30	0.65	146
6		44.66	0.74	268
7		49.38	0.81	425
Rubber A – glass				
No.	F_N [N]	F_{drive} [N]	μ [—]	v [μm s^{-1}]
1	32.86	29.46	0.90	0.10
2		31.56	0.96	0.08
	—			
3	60.72	63.60	1.05	0.08
4		66.14	1.09	370
5		68.52	1.13	374
6		71.22	1.17	610
Rubber A – tile				
No.	F_N [N]	F_{drive} [N]	μ [—]	v [μm s^{-1}]
1	32.86	17.14	0.52	52
2		21.64	0.67	164
3		26.90	0.83	704
4		30.48	0.94	1600
	—			
5	60.72	22.16	0.37	3.46
6		33.62	0.55	80
7		38.50	0.63	136
8		41.16	0.68	176
9		60.12	0.99	2011

Table 2 Experimental conditions for compound B sliding on concrete and glass

Rubber B – concrete				
No.	F_N [N]	F_{drive} [N]	μ [—]	v [μm s^{-1}]
1	32.86	17.74	0.54	11
2		19.46	0.59	20
	—			
3	60.72	43.88	0.72	54
4		49.38	0.81	191

Rubber B – glass				
No.	F_N [N]	F_{drive} [N]	μ [—]	v [μm s^{-1}]
1	32.86	41.12	1.25	13
2		46.10	1.40	94
	—			
3	60.72	55.60	0.92	0.71
4		66.24	1.09	0.77

Table 3 Experimental conditions for PMMA sliding on concrete and tile

PMMA – concrete				
No.	F_N [N]	F_{drive} [N]	μ [—]	v [μm s^{-1}]
1	32.86	14.58	0.44	6.19
2		15.20	0.46	8.74

PMMA – tile				
No.	F_N [N]	F_{drive} [N]	μ [—]	v [μm s^{-1}]
1	32.86	13.80	0.42	83 360
2		14.46	0.44	102 000

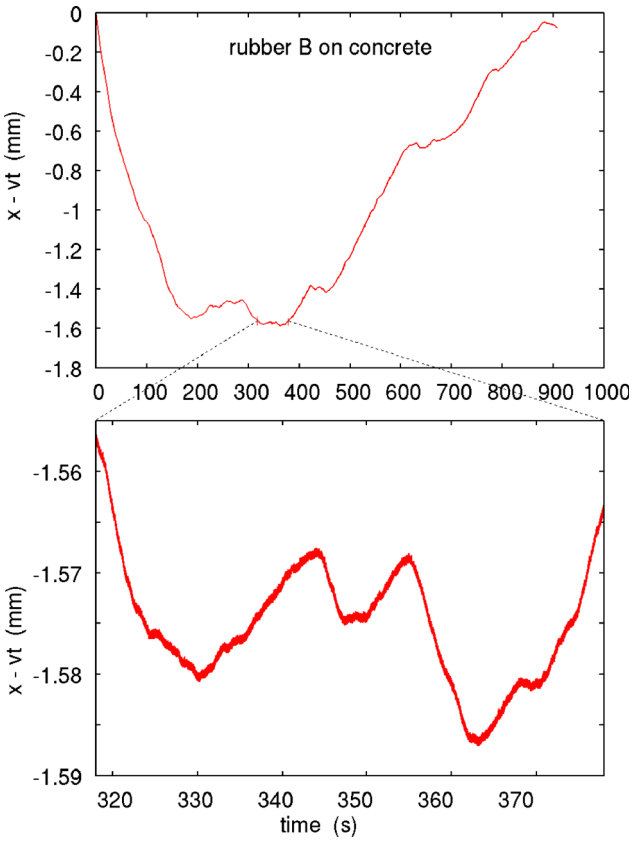

Fig. 8 Top: The noise $\xi(t) = x(t) - vt$ in the large block position as a function of time for sliding of the rubber compound B on concrete. The average velocity v = 0.054 mm s^{-1}. Bottom: A magnified segment.

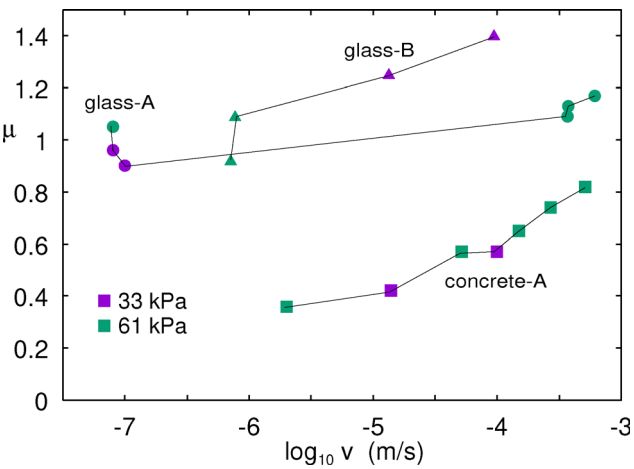

Fig. 9 The friction coefficient as a function of the sliding speed for rubber compound A on a concrete surface (squares) and on a smooth silica glass surface (circles), and for compound B on the glass surface (triangles). The blue and green symbols are for the nominal contact pressures 33 and 61 kPa, respectively.

time ≈900 s. Fig. 8 (bottom) shows the sliding distance for the time segment 318 s to 378 s.

For rubber sliding on a smooth glass surface, we frequently observe highly non-uniform motion, where the sliding speed fluctuates significantly over large distances. Most technological rubbers contain mobile components, such as wax, which can diffuse to the rubber surface. During sliding, the wax film is gradually removed, resulting in slow changes in the friction force. These changes typically occur over sliding distances on the order of 10 cm. In contrast, rubber sliding on a concrete surface exhibits much more stable and reproducible motion, possibly because the concrete asperities can penetrate the wax film.

Fig. 9 presents the (average) friction coefficient as a function of the sliding speed for compound A on concrete (squares) and on the glass surface (circles), and for compound B on the glass surface (triangles). The blue and green symbols correspond to nominal contact pressures of p_0 = 33 kPa and 61 kPa, respectively. Within the experimental noise level, the friction coefficient is independent of the contact pressure, consistent with previous studies. This suggests that the real area of contact is proportional to the normal force, as expected from contact mechanics theory.[8] It also indicates that the contact area is small compared to complete contact and that macroscopic adhesion is absent, which would otherwise lead to a friction coefficient that increases as the pressure p_0 decreases. Although adhesion interactions are always present and contribute to the contact area, they are too weak in this case to manifest macroscopically as a pull-off force.

Consequently, the real contact area vanishes continuously as p_0 approaches zero.[36]

Fig. 10 presents the sliding distance power spectrum $C_x(\omega)$ as a function of frequency for a PMMA block sliding on (a) the concrete and (b) the tile surface. In this system, significant wear occurs, resulting in white powder deposits on the sliding track (see Fig. 11). The slope of the curve in Fig. 10(b) is close to -5, consistent with earlier studies,[16] which found that wear particles at the sliding interface lead to such power spectrum behavior (see also Section 5).

The red and blue lines in Fig. 12 show measured power spectra $C_x(\omega)$ for the rubber compound A on the concrete surface. The theory curve (green line), to be discussed below, has a slope of -4 in the low frequency part of the power spectrum. In Appendix C we present more power spectra for the rubber compound A on concrete, silica glass and the tile surfaces. On concrete we find the exponent $\gamma \approx 4$ and for the glass surface and tile surfaces between 4 and 5. We also present results for rubber compound B on the concrete (where $\gamma \approx 4.3$) and glass (where $\gamma \approx 5$) surfaces.

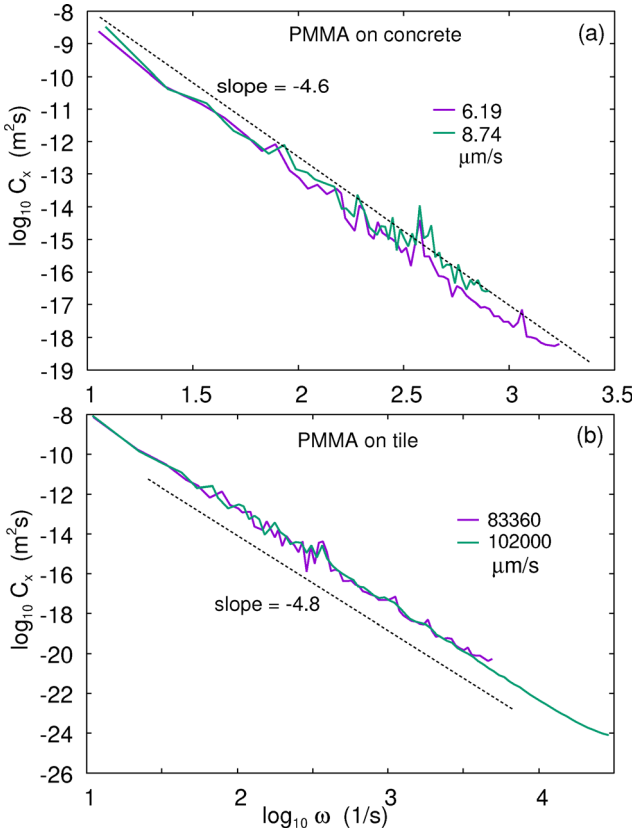

Fig. 10 The sliding distance power spectrum $C_x(\omega)$ as a function of frequency. The experimental result is for a PMMA block sliding on (a) a rough concrete block and (b) a tile surface.

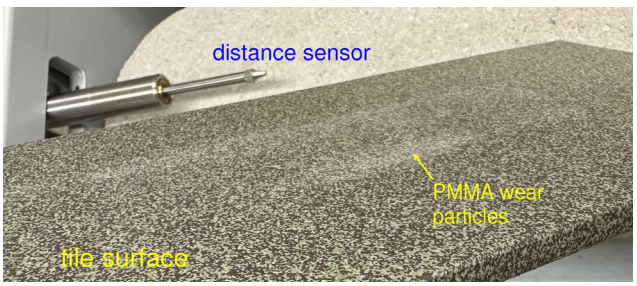

Fig. 11 Wear particles deposited on the tile surface after sliding the PMMA block one time at the speed $v \approx 83$ mm s^{-1} and the normal force $\sim$33 N.

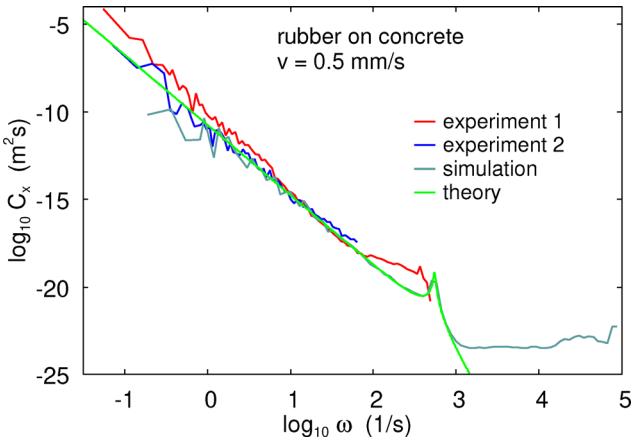

Fig. 12 The sliding distance power spectrum $C_x(\omega)$ as a function of frequency. The experimental result is for rubber compound A sliding on a concrete surface, the theoretical result is for the reference case. Adapted from ref. 19.

10 Comparison of theory with experiment

The experimental data presented in Section 9 shows that the displacement noise power spectra exhibit a power-law behavior of the form $C_x(\omega) \sim \omega^{-\gamma}$ over a wide (low) frequency range, with γ in the range from 4 to 5. The theoretical model predicts a low-frequency exponent of -4 for "clean" surfaces, consistent with observations for rubber A sliding on concrete.

Fig. 12 is adapted from ref. 19, where the displacement noise power spectrum $C_x(\omega)$ for the rubber compound A sliding on the concrete block is compared with the theoretical results (green and gray curves) obtained for the reference case ($N = 30$ miniblocks, $v = 0.5$ mm s^{-1}, $a = 1$ mm, and $\alpha = 0.4$). Note that the experimental data exhibit the same $\sim\omega^{-4}$ scaling as the theoretical curve.

In the simulations, the displacement power spectrum exhibits a high-frequency roll-off caused by the damped oscillations of the miniblocks (see Appendix A). This feature is not observed in the experimental data, likely due to the limited frequency resolution of the current measurement system. Furthermore, to explain measurements performed with higher distance resolution, it may be necessary to extend the theory from the single-length scale model currently used to a multiscale model (see Fig. 1(b)). Thus surface roughness occurs at many length scales, with macroasperities having smaller asperities on top of them. This results in the breakup of macroasperity contact regions

into smaller microasperity contact areas. In our theory, we could model these smaller contact regions with microblocks elastically connected to the miniblocks, as illustrated in Fig. 1(c). The motion of the microblocks generates higher frequency force fluctuations than would arise with only the miniblocks, which could be significant at the higher frequencies not probed in the present experiments.

Friction force fluctuations have also been observed in a study involving an alumina pin sliding on a steel surface.[16] At a constant sliding speed of v = 1 cm s^{-1}, the force power spectrum exhibited a $\sim\omega^{-1}$ dependence at low frequencies, which corresponds to a displacement spectrum $\sim\omega^{-5}$. The authors of ref. 16 attributed this behavior to the presence of wear particles. After these particles were removed, the displacement power spectrum flattened to $\sim\omega^{0}$. This observation is consistent with our experiments for PMMA sliding on tile surfaces, where the exponent is closer to -5. Rubber wear particles are also generated on concrete surfaces,[37,38] but their influence on the displacement noise power spectrum may be smaller, possibly because they become trapped in surface cavities.

It would be of interest to investigate in greater detail the role of wear particles, specifically how their size distribution and concentration influence the slope of the displacement power spectra. One particularly relevant study would involve introducing particles of various sizes into a system that initially exhibits a ω^{-4} spectrum, to examine whether the slope shifts toward ω^{-5}. We plan to carry out such investigations and will report the results in future work.

Another interesting extension of our study would be to investigate how external vibrations may influence the noise spectrum. If the sliding system would be exposed to an external periodic vibration with a frequency that differs from the region where the noise power spectrum $C_x(\omega)$ is studied, then it would show up in the measured data only if it would change the asperity slip dynamics.

Wear particles are crucial for sliding contacts between metals used to transmit electric current.[28] Sliding generally involves wear and irregular fluctuations (noise) of the contact resistance. In ref. 28, the noise in the voltage was measured for different metal–metal contacts under a fixed electric current. While the power spectra of the voltage fluctuations were not shown, the dependence of the rms voltage V_{rms} (which is a frequency integral of the voltage power spectra) on different physical parameters was presented and showed power law behavior.

Rapid events at a sliding interface generate air pressure fluctuations (sound waves). The primary sources of acoustic radiation are believed to be interactions of asperities at the interface and structural vibrations.[17,18] Acoustic noise often originates from forming and breaking surface asperity contacts. For elastically stiff materials, asperity contact regions are typically a few micrometers in size. Breaking and forming asperity contacts act like small hammer strokes at a high rate. Since surface roughness is random, these impacts occur randomly, mechanically exciting the structure. The Fourier transform of a pulse is constant, resulting in a wide noise spectrum.

An important length scale for electric, acoustic, and friction noise is the distance over which the asperity contact population is entirely renewed. If both surfaces have similar roughness, this distance is of the order of the diameter D of the macroasperity contact region. Rabinowicz[39] measured this distance D and found it typically $\sim$10 μm for metallic contacts. Using this one can estimate[17,18] that the noise from breaking and forming asperity contacts typically overlap in time and is perceived as steady-state noise by the human ear.

Sliding friction can also excite vibrational eigenmodes of the contacting solids, generating sound waves. Rayleigh[40] found that when a glass was set ringing by running a moistened finger around its rim, the frequency of the ring matched that of the sound produced when the glass was tapped. He proposed that the ringing was caused by the friction of the finger exciting tangential motion in the glass. However, in this case, the vibrational eigenmodes are most likely not produced by the breaking and forming of asperity contacts, but rather result from stick-slip motion of the finger on the glass surface. This stick-slip behavior is caused by a decrease in friction with increasing sliding velocity, which occurs before full hydrodynamic lubrication is established.[29]

11 Summary and conclusion

We have shown that the stochastic formation and rupture of asperity contacts lead to characteristic displacement noise spectra. While the average friction force remains constant under steady sliding, the instantaneous force fluctuates around this mean value, leading to corresponding fluctuations in the sliding velocity. In this study, we extend the analysis to include additional material combinations (*e.g.*, PMMA on tile) and systematically explore the spectral features of these fluctuations under varying interfacial conditions.

For the case of sliding on rough concrete, the displacement fluctuations of the block exhibit a power spectrum that decays as ω^{-4} over a broad frequency range. As demonstrated in ref. 19, this behavior is well captured by a spring-block model in which fluctuating interfacial forces arise from the stochastic formation and rupture of asperity contact regions.

For sliding on tile and smooth glass surfaces, the exponent of the displacement power spectrum varies between -4 and -5, depending on the block material, compound composition, and experimental conditions. An exponent close to -5, which corresponds to a $\sim\omega^{-1}$ power spectrum of the friction force, appears to result from the presence of contamination layers or wear debris. This behavior is approximated by model III and is further discussed in Appendix B.

The variations in displacement exponents across different surfaces and rubber compounds are attributed to a combined effect of contamination (or wear debris) and different wear mechanisms at the sliding interface. Abrasive wear typically occurs on rough surfaces, whereas smearing is more likely on smooth surfaces. The contribution from wear debris is more pronounced on smooth surfaces, as debris may become trapped in deep valleys or cavities on rough surfaces and thus have less influence. Additionally, wear rates vary with rubber compound composition, which in turn influences the nature of the fluctuations in the sliding motion.

The displacement power spectrum shifts along the frequency axis with varying sliding speeds. This shift can be understood by considering that higher sliding speeds result in more frequent formation and breaking of asperity contacts, effectively compressing the time scale of fluctuations. Thus, as the sliding speed v increases, the entire power spectrum shifts to higher frequencies. Conversely, at lower sliding speeds, the time intervals between asperity interactions increase, causing the power spectrum to shift to lower frequencies.

Building upon our previous study,[19] where the frequency range of displacement measurements was limited by sensor resolution, we have evaluated several commercially available high-resolution displacement sensors. However, their performance did not meet the requirements of our system. We still plan to improve the experimental setup using a displacement sensor with significantly enhanced resolution. This would allow access to much higher frequency components of the block motion and potentially capture the transition from static to kinetic friction with improved temporal resolution, an aspect particularly relevant in the context of earthquake dynamics.

To model this behavior, it may also be necessary to extend the current model to account for the hierarchical nature of real surface roughness, with smaller asperities located on top of larger ones. We plan to investigate this using a hierarchical distribution of sliding blocks, with smaller blocks attached to larger blocks (as illustrated in Fig. 1(c)), and so forth. For many systems, the breakloose friction force depends on the time of stationary contact, *e.g.* due to slow increase in the contact area from (thermally activated) creep motion, or slow (thermally activated) bond formation in the contact area. In the models we studied above there is no such mechanism which could increase the breakloose friction force, but it would be interesting to extend the model to include a strengthening of the contact with the time of stationary contact. This is the physical origin of rate-and-state models of sliding dynamics, which have been found to agree with experimental observations.

Conflicts of interest

The authors have no conflicts to disclose. All authors have contributed equally.

Data availability

Processed power spectrum data are available at Zenodo: **https://doi.org/10.5281/zenodo.15374445**.

Appendices

Appendix A

The equation of motion for the large block

$$M\ddot{x} = F_{\text{drive}} - k_0 \sum_i (x - x_i) - m\eta_0 \sum_i (\dot{x} - \dot{x}_i) \qquad \text{(A1)}$$

and for the miniblocks

$$m\ddot{x}_i = -k_0(x_i - x) - m\eta_0(\dot{x}_i - \dot{x}) - m\eta_1\dot{x}_i - f_{\text{kin}} - f_i(t) \qquad \text{(A2)}$$

without the fluctuating force $f_i(t)$ the motion is steady at the sliding speed v. We write

$$x = x_a + vt + \xi(t)$$

$$x_i = vt + \xi_i(t)$$

where

$$Nk_0x_a = F_{\text{drive}}$$

$$N(m\eta_1 v + f_{\text{kin}}) = F_{\text{drive}}$$

Using these results and taking the Fourier transform of (A2) gives

$$-m\omega^2\xi_i = -k_0(\xi_i - \xi) - i\omega m\eta_0(\xi_i - \xi) - i\omega m\eta_1\xi_i - f_i(\omega)$$

or

$$Q_1(\omega)\xi_i(\omega) = P_1(\omega)\xi(\omega) - f_i(\omega) \qquad \text{(A3)}$$

where

$$Q_1(\omega) = -m\omega^2 + k_0 + i\omega(\eta_0 + \eta_1)$$

$$P_1(\omega) = k_0 + i\omega m\eta_0$$

From (A1) we get

$$-M\omega^2\xi(\omega) = -k_0 \sum_i (\xi - \xi_i) - i\omega m\eta_0 \sum_i (\xi - \xi_i)$$

or

$$Q_0(\omega)\xi(\omega) = P_0(\omega)\frac{1}{N}\sum_i \xi_i(\omega) \qquad \text{(A4)}$$

where

$$Q_0(\omega) = -M\omega^2 + Nk_0 + i\omega Nm\eta_0$$

$$P_0(\omega) = Nk_0 + i\omega Nm\eta_0$$

Combining (A3) and (A4) gives

$$Q_0(\omega)\xi = \frac{P_0(\omega)}{Q_1(\omega)}\left(P_1(\omega)\xi - \frac{1}{N}\sum_i f_i(\omega)\right)$$

$$\xi(\omega) = Z(\omega)\frac{1}{N}\sum_i f_i(\omega) \qquad \text{(A5)}$$

where

$$Z(\omega) = -\frac{P_0(\omega)}{S(\omega)}$$

$$\begin{aligned} S(\omega) &= Q_0(\omega)Q_1(\omega) - P_0(\omega)P_1(\omega) \\ &= \left(-M\omega^2 + Nk_0 + i\omega Nm\eta_0\right)\left(-m\omega^2 + k_0 + i\omega m(\eta_0 + \eta_1)\right) \\ &\quad - (Nk_0 + i\omega Nm\eta_0)(k_0 + i\omega m\eta_0) \end{aligned}$$

For $\omega \ll \omega_c$ we get

$$S(\omega) \approx i\omega mNk_0\eta_1$$

and

$$Z(\omega) \approx -\frac{1}{i\omega m\eta_1} \tag{A6}$$

We will calculate the power spectrum of $\xi(t)$. We assume that the fluctuating forces f_i are uncorrelated so that $\langle f_i(t)f_j(t')\rangle = 0$. We get

$$\frac{1}{N^2}\sum_{ij}\langle f_i(t)f_j(t')\rangle = \frac{1}{N^2}\sum_i\langle f_i(t)f_i(t')\rangle = \frac{1}{N}\langle f(t)f(t')\rangle$$

where $f(t)$ stands for any of the $f_i(t)$. Note that

$$\left\langle f^2(t)\right\rangle = \alpha^2 {f_{\mathrm{kin}}}^2\int_0^1 \mathrm{d}r(r-0.5)^2 = \frac{1}{12}\alpha^2 {f_{\mathrm{kin}}}^2 \tag{A7}$$

The fluctuating force $f(t)$ takes the value u_n for $t_n < t < t_{n+1}$, where both u_n and t_n are random variables but with $\langle t_{n+1} - t_n\rangle = \tau_0$. The Fourier transform of the fluctuating force

$$\begin{aligned} f(\omega) &= \frac{1}{2\pi}\sum_n \frac{u_n}{i\omega}\left(\mathrm{e}^{-i\omega t_n} - \mathrm{e}^{-i\omega t_{n+1}}\right) \\ &= \frac{1}{2\pi}\sum_n \frac{u_n}{i\omega}\mathrm{e}^{-i\omega t_n}\left(1 - \mathrm{e}^{-i\omega(t_{n+1}-t_n)}\right) \end{aligned}$$

The power spectrum of the fluctuating force

$$C_{\mathrm{f}}(\omega) = \frac{2\pi}{T}\left\langle |f(\omega)|^2\right\rangle$$

$$= \frac{1}{2\pi T}\sum_n \left\langle {u_n}^2\right\rangle \frac{2}{\omega^2}(1 - \langle\cos\omega(t_{n+1} - t_n)\rangle) \tag{A8}$$

Here we have used that averaging over u_n and t_n are independent processes and also that $\langle u_n u_m\rangle = \langle u_n\rangle\langle u_m\rangle = 0$ if $n \neq m$. The sum in (A8) is over N' terms where the total sliding time $T = N'a/v$. Each of these terms gives the same result so if we denote $t_{n+1} - t_n = \tau_n$ and use that

$$\left\langle {u_n}^2\right\rangle = \alpha^2 {f_{\mathrm{kin}}}^2\int_0^1 \mathrm{d}r(0.5 - r)^2 = \frac{1}{12}\alpha^2 {f_{\mathrm{kin}}}^2$$

we get

$$C_{\mathrm{f}}(\omega) = \frac{v}{12\pi d}{f_{\mathrm{kin}}}^2\frac{\alpha^2}{\omega^2}(1 - \langle\cos(\omega\tau_n)\rangle)$$

Since $\langle\tau_n\rangle = \tau_0 = a/v$ and since in our applications typically $\omega\tau_0 \gg 1$ the average

$$\langle\cos(\omega\tau_n)\rangle \approx 0$$

To evaluate $\langle\cos(\omega\tau_n)\rangle$ for a general case assume that $\tau_n = \tau$ is a random variable with the average $\langle\tau\rangle = \tau_0$. We get

$$\langle\cos(\omega\tau)\rangle = \frac{1}{2}\left(\left\langle \mathrm{e}^{i\omega\tau}\right\rangle + \left\langle \mathrm{e}^{-i\omega\tau}\right\rangle\right)$$

Using the cumulant expansion truncated at the second order

$$\left\langle \mathrm{e}^{i\omega\tau}\right\rangle = \mathrm{e}^{i\omega\langle\tau\rangle - s^2\omega^2/2}$$

where

$$s^2 = \langle\tau^2\rangle - \langle\tau\rangle^2 = \langle(\tau - \tau_0)^2\rangle$$

Thus we get

$$\langle\cos(\omega\tau)\rangle = \mathrm{e}^{-s^2\omega^2/2}\cos(\omega\tau_0)$$

Using that $\tau = t_1 - t_2$ and that t_1 is a random number uniformly distributed between 0 and τ_0 and t_2 a random number uniformly distributed between τ_0 and $2\tau_0$ we can write $\tau = \tau_0 + \tau_0(r - r')$ where r and r' are uniformly distributed between 0 and 1. Using this gives $s^2 = {\tau_0}^2/6$. Hence for $\omega\tau_0 \gg 1$ we get $\langle\cos(\omega\tau_n)\rangle \approx 0$ and

$$C_{\mathrm{f}}(\omega) \approx \frac{v}{12\pi d}{f_{\mathrm{kin}}}^2\frac{\alpha^2}{\omega^2} \tag{A9}$$

From (A5) we get

$$\begin{aligned} C_x(\omega) &= \frac{2\pi}{T}\left\langle|\xi(\omega)|^2\right\rangle = |Z(\omega)|^2\frac{2\pi}{T}\frac{1}{N}\left\langle|f(\omega)|^2\right\rangle \\ &= |Z(\omega)|^2\frac{1}{N}C_{\mathrm{f}}(\omega) \end{aligned} \tag{A10}$$

For $v/a \ll \omega \ll \omega_c$ we can use (A6), (A9) and (A10) to get

$$C_x(\omega) \approx \frac{\alpha^2}{\omega^4}\frac{v{f_{\mathrm{kin}}}^2}{12\pi Na(m\eta_1)^2} \tag{A11}$$

In the numerical simulations we used $Nf_{\mathrm{kin}} = F_{\mathrm{drive}}/2$ so that $m\eta_1 v = f_{\mathrm{kin}}$. Using this we get

$$C_x(\omega) \approx \frac{\alpha^2}{\omega^4}\frac{v^3}{12\pi Na} \tag{A12}$$

Fig. 13 shows the sliding distance power spectrum $C_x(\omega)$ as a function of frequency for the standard (or reference) parameters. The green curve represents the simulation results, and the violet curve shows the theoretical prediction (A10). The theory agrees well with the simulation results in the overlapping frequency region. The roll-off region is caused by the

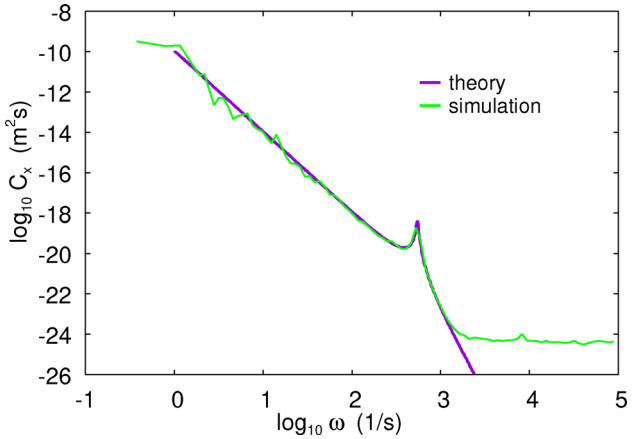

Fig. 13 The sliding distance power spectrum $C_x(\omega)$ as a function of frequency for the standard (or reference) parameters. The green curve is from simulations, and the violet curve is the theory prediction (eqn (A10)).

damped oscillatory motion of the miniblocks when they experience changes in friction with the substrate. This is illustrated in Fig. 14, which shows the sliding distance of the large block as a function of time for a very short time period from the simulation used to obtain Fig. 13. Note the damped oscillations in the center of mass position that occur every time a miniblock experiences a change in the substrate force at random time points t_n. On average, during the time period Δt, the block slides a distance of $v\Delta t$, and for N miniblocks, there will be $Nv\Delta t/a$ changes in the friction. Thus, the average time interval between changes in the friction is $\Delta t = a/Nv$. In the present case, with $N = 30$, $a = 1$ mm, and $v = 0.5$ mm s^{-1}, this gives $\Delta t \approx 0.07$ s, which is consistent with the figure.

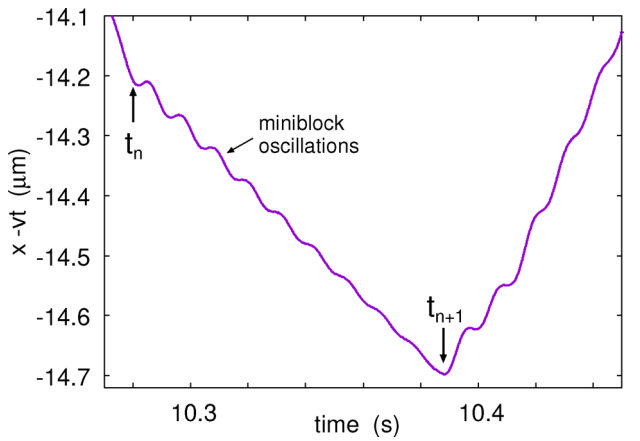

Fig. 14 The sliding distance of the large block as a function of time for a very short time period from the simulation used to obtain Fig. 13. Note the damped oscillations in the center of mass position, which occur every time a miniblock experiences a change in the substrate force at random time points t_n. On average, during the time period Δt, the block slides a distance of $v\Delta t$, and for N miniblocks, there will be $Nv\Delta t/a$ changes in the friction. Thus, the average time interval between changes in the friction is $\Delta t = a/Nv$. In the present case, $N = 30$, $a = 1$ mm, and $v = 0.5$ mm s^{-1}, giving $\Delta t \approx 0.07$ s.

The theory above can be slightly generalized as follows. Let $f_{\rm kin}(\dot{x}_i)$ be the (non-random part) of the kinetic friction force acting on a miniblock from the substrate. Writing $x_i = vt + \xi_i(t)$ we get to first order in ξ_i

$$f_{\rm kin}(\dot{x}) = f_{\rm kin}(v) + f'_{\rm kin}(v)\dot{\xi}_i$$

where $f_{\rm kin}(v)$ was denoted as $f_{\rm kin} + m\eta_1 v$ above and $f'_{\rm kin}(v)$ by $m\eta_1$. In this case, the sliding speed is determined by

$$f_{\rm kin}(v) = F_{\rm drive}/N$$

Using that $m\eta_1 v = v f'_{\rm kin}(v)$ and (A7) we can write (A11) as

$$C_x(\omega) \approx \frac{v^3}{\pi N a \omega^4}\frac{\langle f^2\rangle}{\left[v f'_{\rm kin}(v)\right]^2}$$

Since there is no reason for $v f'_{\rm kin}(v)$ and $\sqrt{\langle f^2\rangle}$ to have the same velocity dependence it is clear that the velocity dependence of $C_x(\omega)$ may be more complex than the $\sim v^3$ predicted by (A10). Thus, for rubber sliding on the concrete surface we find (see Fig. 15) $C_x \sim v^{5/3}$. Assuming that N and a are velocity independent, this gives

$$\frac{\langle f^2\rangle}{\left[v f'_{\rm kin}(v)\right]^2} \sim v^{-4/3}$$

In the studied velocity range the friction force on concrete increases approximately linearly with $\ln v$ (see Fig. 9) so we expect $v f'_{\rm kin}(v)$ to be nearly independent of the velocity which implies that the rms of the fluctuating force, $\sqrt{\langle f^2\rangle}$, acting on a miniblock scales with the velocity roughly as $\sim v^{-2/3}$.

Using (4) and the equations above it is easy to calculate the mean-square (ms) displacement

$$\xi_{\rm rms}{}^2 = 2\int_{\omega_0}^{\omega_1} {\rm d}\omega C_x(\omega) \qquad \text{(A13)}$$

Here ω_0 and ω_1 are the lowest and highest frequency in the problem. We take $\omega_0 = \pi/t_0$ where t_0 is the total sliding time so

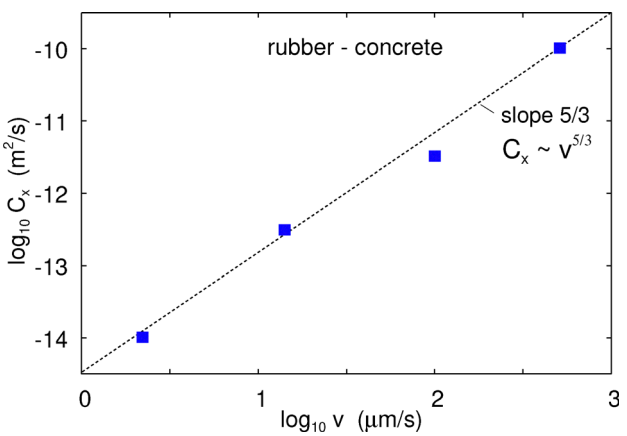

Fig. 15 The velocity dependence of C_x for $\omega \approx 0.4$ s^{-1} for rubber block sliding on concrete surface (log–log scale). The slope of the line is −5/3 corresponding to $C_x \sim v^{-5/3}$.

that $vt_0 = L_0$ is the sliding distance. The highest frequency is taken as ω_c but the exact value is not very important since it turns out the most important contribution to the integral in (A13) is from $\pi/t_0 < \omega < 1/\tau_0$. For these ω we can expand

$$\langle \cos(\omega\tau)\rangle \approx 1 - \frac{1}{2}\omega^2\langle\tau^2\rangle$$

In this frequency region (A12) must be multiplied by the factor $\omega^2\langle\tau^2\rangle/2$ giving

$$C_x(\omega) \approx \frac{\alpha^2}{\omega^2}\frac{v^3\langle\tau^2\rangle}{24\pi Na}$$

Using this in (A13) gives

$$\xi_{\rm rms}{}^2 \approx \frac{\alpha^2}{\omega_0}\frac{v^3\langle\tau^2\rangle}{12\pi Na} = \frac{7}{72\pi^2}\frac{L_0 a}{N}$$

or $\xi_{\rm rms} \approx 0.1\sqrt{(L_0 a/N)}$. As expected from random walk arguments the rms displacement away from the sliding distance $L_0 = vt$ scales as the square root of the sliding distance.

Thus if a distance increases with $a + b(0.5 - r)$, where r is a random number between 0 and 1, at time points separated by τ then after $n + 1$ time steps the length $x_{n+1} = x_n + a + b(0.5 - r)$. We get $\langle x_{n+1}\rangle = \langle x_n\rangle + a$ and hence $\langle x_n\rangle = na$. Writing $x_n = na + \xi_n$ we get $\xi_{n+1} = \xi_n + b(0.5 - r)$ giving

$$\langle \xi_{n+1}{}^2\rangle = \langle \xi_n{}^2\rangle + b^2\left\langle (0.5 - r)^2\right\rangle = \langle \xi_n{}^2\rangle + \frac{b^2}{12}$$

Iterating this gives

$$\langle \xi_n{}^2\rangle = \frac{nb^2}{12} = \frac{L_0}{a}\frac{b^2}{12}$$

Appendix B

We present a simple model of the contribution of wear particles to the fluctuations in the friction force. Assume that there are N wear particles that perform irregular motion at the sliding interface. We write the friction force as $F_x(t) = F_0 + F_1(t)$ where the ensemble-average of the fluctuating force $F_1(t)$ vanish. We have

$$F_1 = \sum_n f_n(t)$$

where f_n is the force on the block from the wear particle n (with $n = 1, \ldots, N$). The condition $\langle F_1(t)\rangle = 0$, where $\langle\ldots\rangle$ stand for ensemble average, is satisfied if we choose $\langle f_n(t)\rangle = 0$. We assume no interaction between the wear particles so that $\langle f_m(t) f_n(t')\rangle = \langle f_m(t)\rangle\langle f_n(t')\rangle = 0$ if $m \neq n$. This gives

$$C_{\rm F}(\omega) = \frac{2\pi}{T}\left\langle |F_1(\omega)|^2\right\rangle = \frac{2\pi}{T}\sum_n \left\langle |f_n(\omega)|^2\right\rangle$$

We assume that $f_n(t)$ takes the value c_{n1} if $t_1 < t < t_2$, and c_{n2} when $t_2 < t < t_3$ and so on. Here c_{nj} (j odd number) is determined by the friction force acting on the block from the particle n when trapped on the substrate surface and c_{nj} (j even) when sliding relative to the substrate. We get

$$f_n(\omega) = \frac{1}{2\pi}\sum_j \frac{c_{nj}}{i\omega}e^{-i\omega t_j}\left(1 - e^{-i\omega\tau_{nj}}\right) \quad \text{(B1)}$$

where $\tau_{nj} = t_{j+1} - t_j$. We assume that $t_j - t_k$ are random variables which is reasonable since the trapping and releasing of a particle depends on the surface roughness of the two solids (see Fig. 3) which is assumed to be random.

We consider first so large frequencies ω that in general $\omega|t_j - t_k| > 2\pi$ when $j \neq k$. In this case, we get from (B1)

$$\sum_n \left\langle |f_n(\omega)|^2\right\rangle \approx \frac{2}{(2\pi)^2}\sum_{nj}\frac{c_{nj}{}^2}{\omega^2}$$

which gives $C_{\rm F} \sim \omega^{-2}$ and $C_x \sim \omega^{-6}$. The situation for small ω is more complex and the exponent β in the frequency dependence of the force power spectrum, $C_{\rm F} \sim \omega^{-\beta}$, where $\beta = 4\text{-}\gamma$, could be a non-integer as observed in some of the experiments presented in Section 8.

For arbitrary frequency, we get from (B1)

$$\sum_n \left\langle |f_n(\omega)|^2\right\rangle = \frac{2}{(2\pi)^2}\sum_{nj}\frac{c_{nj}{}^2}{\omega^2}\left(1 - \cos\left(\omega\tau_{nj}\right)\right)$$

If we assume that τ_{nj} (n fixed) are random variables with the average τ_{An} when trapped and τ_{Bn} when sliding we can write $T = N_n'(\tau_{An} + \tau_{Bn})$ where N_n' is the number of times the particle n is trapped (or released) during the time T. Using this we get

$$\begin{aligned} C_{\rm F}(\omega) &= \frac{2\pi}{T}\sum_n \left\langle |f_n(\omega)|^2\right\rangle \\ &= \frac{1}{\pi}\sum_n \frac{c_{An}{}^2}{\omega^2(\tau_{An} + \tau_{Bn})}\left(1 - e^{-s_{An}{}^2\omega^2/2}\cos(\omega\tau_{An})\right) \\ &\quad + \frac{1}{\pi}\sum_n \frac{c_{Bn}{}^2}{\omega^2(\tau_{An} + \tau_{Bn})}\left(1 - e^{-s_{Bn}{}^2\omega^2/2}\cos(\omega\tau_{Bn})\right) \end{aligned}$$

where

$$c_{An}{}^2 = \frac{1}{N_n'}\sum_{j\ \rm odd} c_{nj}{}^2, \quad c_{Bn}{}^2 = \frac{1}{N_n'}\sum_{j\ \rm even} c_{nj}{}^2$$

and

$$s_{An}{}^2 = \langle \tau_{An}{}^2\rangle - \langle\tau_{An}\rangle^2$$

and similar for $s_{Bn}{}^2$.

In most cases, there will be a large number of wear particles of different sizes (and shapes). Let us number the particles after increasing size where $n = 1$ is the smallest and $n = N$ is the biggest. It is natural that particles with different sizes will have different relaxation times τ_n so we can write

$$N = \sum_n \to \int {\rm d}n = \int {\rm d}\tau \frac{{\rm d}n}{{\rm d}\tau}$$

Defining the probability of relaxation times by

$$P(\tau) = \frac{1}{N}\frac{\mathrm{d}n}{\mathrm{d}\tau}$$

then

$$\int_0^\infty \mathrm{d}\tau P(\tau) = 1$$

In the present case, we have two relaxation processes, one associated with leaving the trapped state with the probability distribution $P_A(\tau)$ and one associated with going from the sliding state into the trapped state with the probability distribution $P_B(\tau)$. Hence we need to replace

$$\sum_n \rightarrow N\int_0^\infty \mathrm{d}\tau\mathrm{d}\tau' P_A(\tau)P_B(\tau')$$

Using this and denoting ${c_{An}}^2 = {c_A}^2(\tau)$ and similar for ${c_{Bn}}^2$ we can write

$$\begin{aligned} C_F(\omega) &= \frac{N}{\pi}\int_0^\infty \mathrm{d}\tau\mathrm{d}\tau' \frac{P_A(\tau)P_B(\tau')}{\omega^2(\tau+\tau')} \\ &\times \left[{c_A}^2(\tau)\left(1 - \mathrm{e}^{-\alpha\tau^2\omega^2/2}\cos(\omega\tau)\right)\right. \\ &\left. + {c_B}^2(\tau')\left(1 - \mathrm{e}^{-\alpha{\tau'}^2\omega^2/2}\cos(\omega\tau')\right)\right] \end{aligned} \quad \text{(B2)}$$

where we have assumed ${s_n}^2 = \alpha{\tau_n}^2$. If

$$P_A(\tau){c_A}^2(\tau) \sim \tau^{-\beta}, \quad P_B(\tau){c_B}^2(\tau) \sim \tau^{-\beta'}$$

then from (B1) $C_F(\omega) \sim \omega^{\beta+\beta'-3}$. For $\beta + \beta' = 2$ this gives $C_F(\omega) \sim \omega^{-1}$. This is similar to the ω^{-1} "flicker noise" in vacuum tubes (and other electronic devices) which is usually explained as resulting from a set of trapping sites with different (release) relaxation times. For flicker noise one can argue[41] for why the probability distribution of relaxation times is such as to give a ω^{-1} noise but for the friction case we have no argument for why $\beta + \beta'$ should equal to 2.

Appendix C

Here we present the power spectra for compound A on the concrete, silica glass and tile surfaces and for rubber compound B on the concrete and glass surfaces.

Fig. 16 shows the sliding distance power spectrum $C_x(\omega)$ as a function of frequency for rubber compound A sliding on (a) the concrete block, (b) the silica glass plate, and (c) the tile surface, at different sliding speeds. In all cases, the slope of the curves ranges from -4 to -5, with the slope for the concrete surface being approximately -4. This indicates that the low-frequency power spectra in these cases are approximately proportional to ω^{-4}.

For compound A sliding on the glass surface at high sliding speeds, the distance power spectrum exponent is approximately -4.75, whereas at low sliding speeds, it matches that observed for the concrete surface. Additional measurements on the smooth glass surface using another rubber compound (compound B) showed a displacement exponent of approximately -5, as shown in Fig. 17(b). This suggests that different interfacial processes may occur on the glass surface compared to the concrete surface.

Fig. 16(c) shows the sliding distance power spectrum $C_x(\omega)$ as a function of frequency for rubber compound A sliding on a tile surface. The slope of the curve is close to -4 at high sliding speeds and -5 at low sliding speeds.

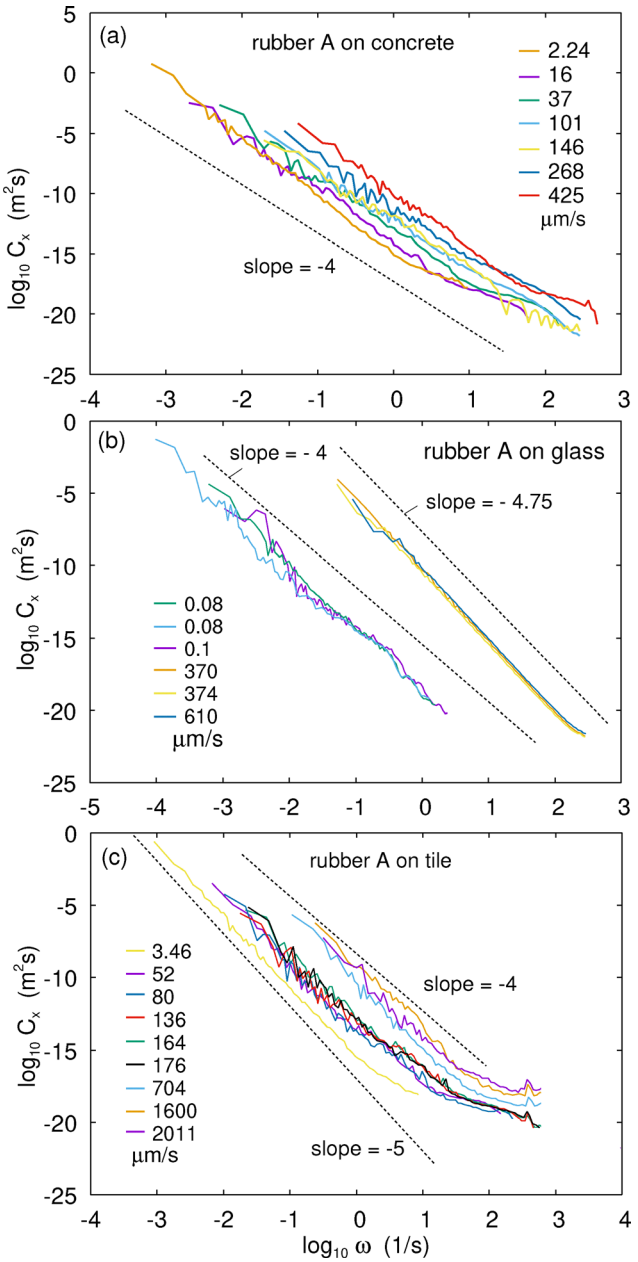

Fig. 16 The power spectrum of the sliding displacement $C_x(\omega)$ as a function of frequency for rubber blocks (compound A) sliding on (a) a rough concrete block, (b) a smooth silica glass plate, and (c) a tile surface, at different sliding speeds as indicated. The experimental data shown in (a) and (b) were originally presented in ref. 19 and are included here for reference and for comparison with the new systems studied.

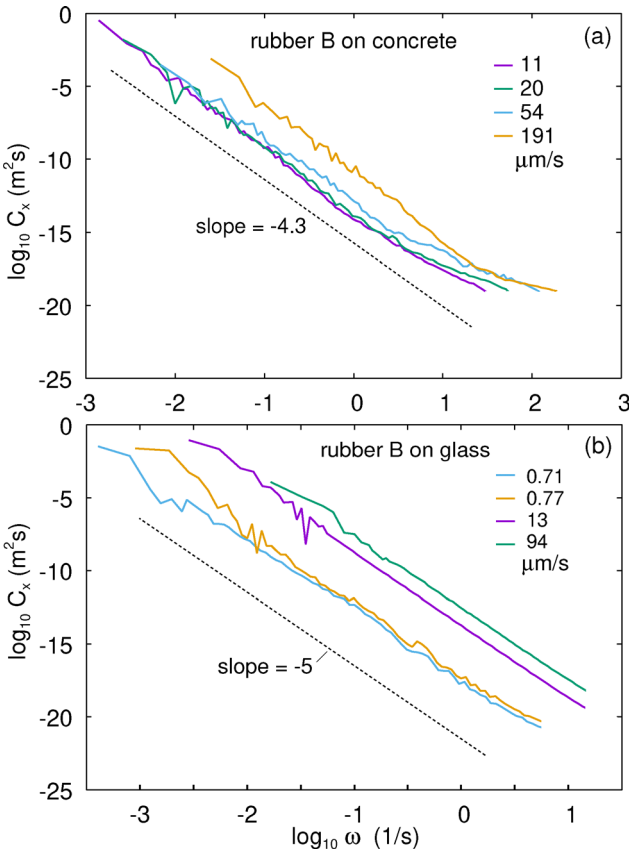

Fig. 17 The sliding distance power spectrum $C_x(\omega)$ as a function of frequency for rubber blocks (compound B) sliding on (a) a rough concrete block and (b) a smooth silica glass plate, at different sliding speeds indicated.

Acknowledgements

This work was supported by the Strategic Priority Research Program of the Chinese Academy of Sciences, Grant No. XDB0470200.

References

1 B. Persson, On the fractal dimension of rough surfaces, *Tribol. Lett.*, 2014, **54**, 99.
2 P. Nayak, Random process model of rough surfaces, *J. Lubr. Technol.*, 1971, **93**, 398.
3 R. Aghababaei, E. Brodsky, J. Molinari and S. Chandrasekar, How roughness emerges on natural and engineered surfaces, *MRS Bull.*, 2022, **47**, 12.
4 B. Persson, *Sliding Friction: Physical Principles and Applications*, Springer, Heidelberg, 2000.
5 E. Gnecco and E. Meyer, *Elements of Friction Theory and Nanotribology*, Cambridge University Press, Cambridge, 2015.
6 J. Israelachvili, *Intermolecular and Surface Forces*, Academic Press, London, 3rd edn, 2011.
7 J. Barber, *Contact Mechanics (Solid Mechanics and Its Applications)*, Springer, 2018.
8 B. Persson, Contact mechanics for randomly rough surfaces, *Surf. Sci. Rep.*, 2006, **61**, 201.
9 B. Persson, Theory of rubber friction and contact mechanics, *J. Chem. Phys.*, 2001, **115**, 3840.
10 B. Persson, O. Albohr, U. Tartaglino, A. Volokitin and E. Tosatti, On the nature of surface roughness with application to contact mechanics, sealing, rubber friction and adhesion, *J. Phys.: Condens. Matter*, 2005, **17**, R1.
11 M. Rozman, M. Urbakh and J. Klafter, Origin of stick-slip motion in a driven two-wave potential, *Phys. Rev. E: Stat. Phys., Plasmas, Fluids, Relat. Interdiscip. Top.*, 1996, **54**, 6485.
12 C. Yan, H. Chen, P. Lai and P. Tong, Statistical laws of stick-slip friction at mesoscale, *Nat. Commun.*, 2023, **14**, 6221.
13 M. Müser, How static is static friction?, *Proc. Natl. Acad. Sci. U. S. A.*, 2008, **105**, 13187.
14 M. Müser, Velocity dependence of kinetic friction in the Prandtl-Tomlinson model, *Phys. Rev. B: Condens. Matter Mater. Phys.*, 2011, **84**, 125419.
15 S. Shi, M. Wang, Y. Poles and J. Fineberg, How frictional slip evolves, *Nat. Commun.*, 2023, **14**, 8291.
16 M. Duarte, I. Vragovic, J. Molina, R. Prieto, J. Narciso and E. Louis, 1/*f* Noise in Sliding Friction under Wear Conditions: The Role of Debris, *Phys. Rev. Lett.*, 2009, **102**, 045501.
17 M. Mohamed, G. Ahmadi and F. Loo, A Study on the Mechanics of Fatigue-Dominated Friction Noise, *J. Vib. Acoust.*, 1990, **112**, 222.
18 A. Bot, Noise of sliding rough contact, *J. Phys.: Conf. Ser.*, 2017, **797**, 012006.
19 R. Xu, F. Zhou and B. Persson, Brownian friction dynamics: Fluctuations in sliding distance, *Phys. Rev. E*, 2024, **110**(6), L062801.
20 LIGO; Accessed: YYYY-MM-DD. **https://www.ligo.caltech.edu**.
21 J. Carlson and J. Langer, Mechanical model of an earthquake fault, *Phys. Rev. A: At., Mol., Opt. Phys.*, 1989, **40**, 6470.
22 J. Dieterich, *Modeling of rock friction: 1.* Experimental results and constitutive equations, *J. Geophys. Res.*, 1979, **84**, 2161.
23 A. Ruina, Slip instability and state variable friction laws, *J. Geophys. Res.: Solid Earth*, 1983, **88**, 359.
24 W. Steinhardt and E. Brodsky, Seismological Stress Drops for Confined Ruptures Are Invariant to Normal Stress, *Geophys. Res. Lett.*, 2023, **50**, e2022GL101366.
25 W. Steinhardt and E. Brodsky, Precursory Locking Precedes Slip Events on Laboratory Fault, *Geophys. Res. Lett.*, 2025, **52**, e2024GL112882.
26 G. Wu, K. Dong, Z. Xu, S. Xiao, W. Wei and H. Chen, *et al.*, Pantograph–catenary electrical contact system of high-speed railways: recent progress, challenges, and outlooks, *Railw. Eng. Sci.*, 2022, **30**, 437.
27 M. Taniguchi, T. Inoue and K. Mano, The frequency spectrum of electrical sliding contact noise and its waveform model, *IEEE Trans. Compon., Hybrids, Manuf. Technol.*, 1985, **8**(3), 366–371.
28 K. Tsuchiya and T. Tamai, Fluctuations of contact resistance in sliding contact, *Wear*, 1970, **16**, 337.

29 R. Spurr, The ringing of wine glasses, *Wear*, 1961, **4**, 150.
30 B. Persson, Theory of friction: Stress domains, relaxation, and creep, *Phys. Rev. B: Condens. Matter Mater. Phys.*, 1995, **51**, 13568.
31 W. Schottky, Small-Shot Effect and Flicker Effect, *Phys. Rev.*, 1926, **28**, 74.
32 J. Bernamont, Fluctuations de potential aux bornes d'un conducteur metallique de faible volume parcouru par un courant, *Ann. Phys.*, 1937, **7**, 71.
33 A. McWhorter, in *1/f noise and germanium surface properties*, ed. R. Kingston, University of Pennsylvania Press, Philadelphia, 1957, pp. 207–228.
34 L. Jakobsen, A. Tiwari, I. Sivebaek and B. Persson, Footwear soles friction on steel and tile surfaces: experiments and modeling, *Friction*, 2025, **13**(1).
35 T. Tolpekina and B. Persson, Adhesion and friction for three tire tread compounds, *Lubricants*, 2019, **7**(3), 20.
36 B. Persson, I. Sivebaek, V. Samoilov, K. Zhao, A. Volokitin and Z. Zhang, On the origin of Amonton's friction law, *J. Phys.: Condens. Matter*, 2008, **20**, 395006.
37 B. Persson, R. Xu and N. Miyashita, *Rubber wear: Experiment and theory*, 2024. Manuscript in preparation.
38 R. Xu, N. Miyashita and B. Persson, Rubber wear on concrete: Dry and in-water conditions, *Wear*, 2024, **578–579**, 206200.
39 E. Rabinowicz, The Nature of the Static and Kinetic Coefficients of Friction, *J. Appl. Phys.*, 1951, **22**, 1373.
40 J. Rayleigh, *The theory of sound*, Macmillan, London, vol. 2, 1896.
41 P. Dutta and P. Horn, *Low-frequency fluctuations in solids*: 1/*f noise*, *Rev. Mod. Phys.*, 1981, **53**, 497.